Modeling Air Entrainment Rate and Aeration Efficiency of Weirs Using ANN Approach

Ahmet BAYLAR [1♠], Ozgur KISI [2], M. Emin EMIROGLU [1]

[1] *Firat University, Civil Engineering Department, Elazig, Turkey*

[2] *Erciyes University, Civil Engineering Department, Kayseri, Turkey*

ABSTRACT

The concentration of dissolved oxygen is an important indicator of water quality because aquatic life lives on the dissolved oxygen in the water. A free overfall jet from a weir plunging into downstream water causes entrainment of the air bubbles if the free overfall jet velocity exceeds a certain critical value and hence aeration occurs. This paper investigates the free overfall jets from triangular sharp−crested weirs and their effect on the air entrainment rate and the aeration efficiency. The artificial neural network models, multi nonlinear and linear regression equations were obtained for the triangular sharp−crested weirs relating the air entrainment rate and the aeration efficiency to drop height, discharge, and angle in triangular sharp−crested weir. There were good agreements between the measured values and the values obtained using the artificial neural network and multi nonlinear regression models.

Key Words: *Air entrainment rate, Aeration efficienc,; Dissolved oxygen; Weir, Neural networks.*

1. INTRODUCTION

Water can hold a limited amount of oxygen. That is determined by atmospheric pressure, temperature and salinity. In a natural setting, oxygen is added to water by atmospheric diffusion at the surface, by wind circulation (augmented surface diffusion) and by photosynthesis (oxygen produced by phytoplankton or algae). Photosynthesis accounts for most of the oxygen in water. The oxygen content of water increases with increasing atmospheric pressure and decreasing temperature and salinity. The amount of oxygen in water is measured as milligrams per liter (mg/L) dissolved oxygen (DO).

The level of dissolved oxygen is one of the best indicators of overall water quality. Oxygen is a necessary element to all forms of life. Adequate oxygen levels are necessary to provide for aerobic life forms which carry on natural stream purification processes. As dissolved oxygen levels in water drop below 5.0 mg/L, aquatic life is put under stress. The lower the concentration, the greater the stress. Oxygen levels that remain below 1−2 mg/L for a few hours can result in large fish kills. Total dissolved oxygen concentrations in water should not exceed 110 percent. Concentrations above this level can be harmful to aquatic life.

The physical process of oxygen transfer from the atmosphere acts to replenish the used oxygen. This process has been termed aeration. Hydraulic structures increase the amount of dissolved oxygen in a river system, even though the water is in contact with the structure for only a short time. The same quantity of oxygen transfer that normally would occur over several kilometers in a river can occur at a single hydraulic structure. The primary reason for this accelerated oxygen transfer is that air is entrained into the flow in the form of a large number of bubbles. These air bubbles greatly increase the surface area available for mass transfer.

Wilhelms et al. [1], Chanson [2], Ervine [3], and Gulliver et al. [4] reviewed studies about aeration efficiency of hydraulic structures. Recently, Baylar and Bagatur [5], Baylar and Bagatur [6,7], Baylar et al. [8,9], Baylar [10], Baylar and Emiroglu [11] and Baylar and Bagatur [12] investigated sharp−crested weirs having different cross−sectional geometry and demonstrated that the air entrainment rate and the aeration efficiency of weirs changed depending on weir

---

♠Corresponding author, e-mail: abaylar@firat.edu.tr

shapes. Results pointed that the air entrainment rate and the aeration efficiency of the triangular sharp−crested weirs are significantly better than for the other sharp−crested weir types. Therefore, the triangular sharp−crested weirs can be used as highly effective aerators in streams, rivers, constructed channels, fish hatcheries, water treatment plants, etc.

In this paper, artificial neural network (ANN) models and regression equations that were developed to determine the air entrainment rate and the aeration efficiency of the triangular sharp−crested weirs were compared to each others.

2. BUBBLE GENERATION MECHANISMS BY FREE OVERFALL JETS

Gameson [13] demonstrated three phases of oxygen transfer for a free overfall jet plunging into a receiving pool. These are (1) in the free overfall jet itself during fall – this is regarded as small; (2) via the free surface of the receiving water – this depends on the intensity of surface agitation in the receiving pool; (3) in the air−water biphasic flow that exists within the receiving pool because of air entrainment – this phase is governed by the air entrainment rate and the bubble contact time in the water. Gameson [13] observed that the last phase was the most significant contributor to the oxygenation process.

The mechanisms by which air is entrained and transferred into water because of a free overfall jet are several and complex. Ervine et al. [14] described four basic air entrainment mechanisms with reference to circular water jets. Tsang [15] adapted these to the current observations of free overfall jets from normal and parallel weirs. Tsang [15] classified mechanisms of air entrainment as: 1− smooth; 2− rough; 3− oscillating; and 4− disintegrated. A description of these stages is given in the following.

Type 1: This results largely from smooth, solid jets. The major source of air supply is visualized as a thin layer surrounding the jet and carried into the water upon impact, and therefore air entrainment capacity is limited. The water surface in the receiving pool is relatively undisturbed.

Type 2: This results from rough, solid jets. The air supply can be considered as coming largely from small air pockets entrapped between the jet surface roughness and the receiving water. At impact, the jet produces ripples on the receiving pool surface. Compared to the Type 1 mechanism under similar conditions, this results in shallower bubble penetration depth but increased entrainment rate, because the bubbles are more densely packed in the biphasic zone.

Type 3: This results from oscillating jets and those approaching disintegration. The primary air source originates from large air pockets entrapped between the undulating jet and the receiving pool surface. The receiving pool surface is considerably agitated, and air may also be entrained by surface roller and splashing.

Large air pockets are transported from the surface into the water and broken down due to turbulence.

Type 4: This results from disintegrated jets. The receiving pool surface is intensely agitated, and air is entrained by the action of surface rollers and by engulfing air pockets as jet fragments hit the receiving pool surface. The bubbles are generally only transported to relatively shallow depths. Disintegrated jets have the advantage over solid jets of greater surface area; however, air entrainment rate and bubble penetration are significantly reduced because of energy loss to the surrounding atmosphere during fall [16].

3. AERATION EFFICIENCY

The change in oxygen concentration over time in a parcel of water as the parcel travels through a hydraulic structure can be expressed as:

$$V \frac{dC}{dt} = k_L A (C_s - C) \quad (3.1)$$

where k_L = bulk liquid film coefficient. The values of C_s and C are the saturation concentration of oxygen in water at prevailing ambient conditions and the actual concentration of oxygen in the water at time t−difference being proportional to the concentration gradient. The term A is the air−water contact area and V is the volume of water associated with this. Eq. (3.1) does not consider sources and sinks of oxygen in the water body because their rates are relatively slow compared to the oxygen transfer that occurs at most hydraulic structures due to the increase in free−surface turbulence and the large quantity of air that is normally entrained into the flow.

The predictive relations assume that C_s is constant and determined by the water−atmosphere partitioning. If that assumption is made, C_s is constant with respect to time, and the oxygen transfer efficiency (aeration efficiency), E may be defined as [4]:

$$E = \frac{C_d - C_u}{C_s - C_u} \quad (3.2)$$

where u and d = subscripts indicating upstream and downstream locations, respectively.

A value of E > 1 means the downstream water has become supersaturated (i.e., $C_d > C_s$). A transfer efficiency value of 1.0 means that the full transfer up to the saturation value has occurred at the structure. No transfer would correspond to E = 0.0. The saturation concentration in distilled, deionized water may be obtained from charts or equations. This is an approximation because the saturation DO concentration for natural waters is often different from that of distilled, deionized water due to the impact of trace contaminants and salinity.

Oxygen transfer efficiency is sensitive to water temperature, and investigators have typically employed a temperature correction factor. For hydraulic structures, the most often used temperature correction factor has been that of Gameson et al. [17], although some investigators have chosen to use an

Arrhenius−type of water temperature correction [18]. Gulliver et al. [19] applied the theories of Levich [20], Hinze [21], and Azbel [22] to mass transfer similitude and developed the relationship:

$$1 - E_{20} = (1 - E)^{1/f} \qquad (3.3)$$

where E = aeration efficiency at the water temperature of measurement; E_{20} = aeration efficiency at the 20 °C; and f = the exponent described by

$$f = 1.0 + 0.02103(T-20) + 8.261 \times 10^{-5}(T-20)^2 \qquad (3.4)$$

where T = water temperature.

4. EXPERIMENTAL PROCEDURES

The data used in this study were taken from study conducted by Baylar and Bagatur [12] on a large model.

Schematic representation of the experimental setup is shown on Figure. 1. The experimental channel was 3.40 m long, 0.60 m wide, and 0.50 m deep with a maximum water flow rate of 4 L/s. The water was pumped from a pump to the stilling tank. The water jet from the test weir plunged into a downstream water pool, whose height could be adjusted using a pulley arrangement. The water depth in the downstream water pool was controlled by an adjustable weir. The plan-view dimensions of the downstream water pool were 1.20 x 1.20 m. An air flow meter installed on the air-hood was used to measure air entrainment rate Q_A. The plan-view dimensions of the air-hood were 0.75 x 0.60 m. The test weir featured three exchangeable weir elements: 45° triangular sharp-crested weir, 90° triangular sharp-crested weir and 135° triangular sharp-crested weir.
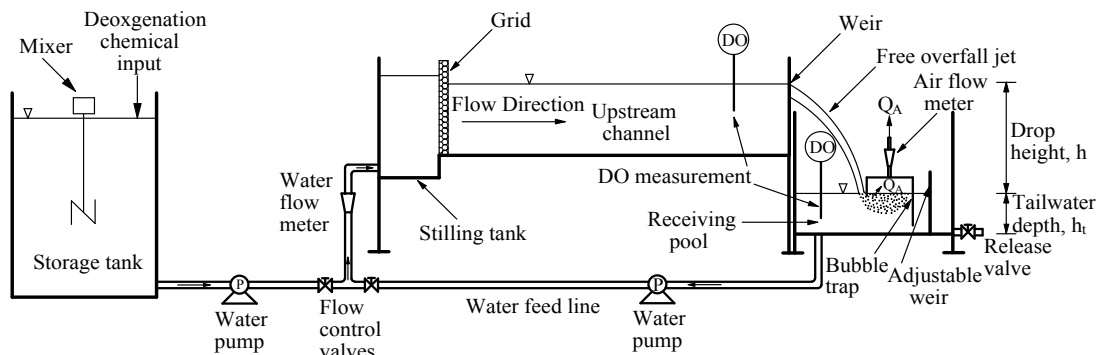

Figure 1. General view of experimental setup.

Each triangular sharp-crested weir was tested under flow rates Q varying from 1.0 to 4.0 L/s in 1.0 L/s steps. The drop height h, defined as the difference between the water levels upstream and downstream of the triangular sharp-crested weir, was varied between 0.15 to 0.90 m in 0.15 m steps. Free overfall jet from the triangular sharp-crested weir plunged through the atmosphere, impinged on the downstream water pool below and entrained air bubbles which were in turn trapped in the air-hood. Then, Q_A was measured by means of the air flow meter installed on the air-hood.

During the experiments, DO measurements upstream and downstream of the weirs were taken using calibrated portable HANNA Model HI 9142 oxygen meters at the locations identified in Figure 1. The DO meter was calibrated daily, prior to use, by the air calibration method. Calibration procedures followed those recommended by the manufacturer. The calibration was performed in humid air under ambient conditions. Each experiment was started by filling thestorage tank and adding Na_2SO_3 and $CoCl_2$ to increase the upstream DO deficit ($C_s - C_u$). The stirrer was installed in the storage tank to ensure accurate and reproducible water-phase measurements.

The residence time of entrained air bubbles in a water body directly affects aeration efficiency. The residence time is related to the bubble flow path and hence bubble penetration depth, D_P, of the bubbles produced by the

overfall jet, which was defined as the vertical distance from the water surface to the lower end of the submerged biphasic region in the water. Aeration and oxygen transfer will increase with air bubble penetration until buoyancy prevails and bubbles rise. In all of the experiments for all weirs, flow paths of entrained air bubbles in the receiving pool were uninterrupted, i.e., the receiving pool depth (tailwater depth) was greater than the bubble penetration depth.

5. RESULTS OF EXPERIMENTS

The results indicate that drop height and discharge are important parameters influencing the air entrainment rate Q_A. Q_A increased with increasing drop height and discharge in all triangular sharp-crested weirs. The reason of this can be explained with the increased momentum of the jet flow and the increased jet surface roughness due to the increased jet expansion. 45° and 90° triangular sharp-crested weirs were found to have the higher values of Q_A than 135° triangular sharp-crested weir. The primary reason for these differences in Q_A can be found by variation in the geometry of the jet. The geometry of the jet was dependent on angle in triangular sharp-crested weir θ. The expansion of the free overfall jet depending on θ was greater in 45° and 90° triangular sharp-crested weirs than that of 135° triangular sharp-crested weir. Thus, this led to the greater values of Q_A for 45° and 90° triangular sharp-crested weirs than 135° triangular sharp-crested weir.

Experiments with all triangular sharp-crested weirs indicate that drop height is important factor influencing aeration efficiency E_{20}. It was observed an increase in E_{20} with drop height. Generally, a bigger drop height leads to greater bubble penetration depths into the downstream water pool and longer contact times t_c. This increases E_{20}. Generally, E_{20} reduced as the discharge increased over the whole range of drop heights tested. E_{20} was greatest with 45° triangular sharp-crested weir because in this weir air entrainment which will contribute to the oxygen transfer were greater than the other triangular sharp-crested weirs.

6. ARTIFICIAL NEURAL NETWORKS (ANN)

Artificial neural networks (ANNs) are based on the present understanding of biological nervous system, though much of the biological detail is neglected. ANNs are massively parallel systems composed of many processing elements connected by links of variable weights. Of the many ANN paradigms, the multi-layer backpropagation network (MLP) is by far the most popular [23]. The network consists of layers of parallel processing elements, called neurons, with each layer being fully connected to the proceeding layer by interconnection fully connected to the proceeding layer by interconnection strengths, or weights, W. Figure 2 illustrates a three-layer neural network consisting of layers i, j, and k, with the interconnection weights W_{ij} and W_{jk} between layers of neurons. Initial estimated weight values are progressively corrected during a training process that compares predicted outputs to known outputs, and backpropagates any errors (from right to left in Figure. 2) to determine the appropriate weight adjustments necessary to minimize the errors. The Levenberg-Marquardt (LM) training algorithm was used here for adjusting the weights. The adaptive learning rates were used for the purpose of faster training speed and solving local minima problem. For each epoch, if performance decreases toward the goal, then the learning rate is increased by the factor learning increment. If performance increases, the learning rate is adjusted by the factor learning decrement. The numbers of hidden layer neurons were found using simple trial-error method.
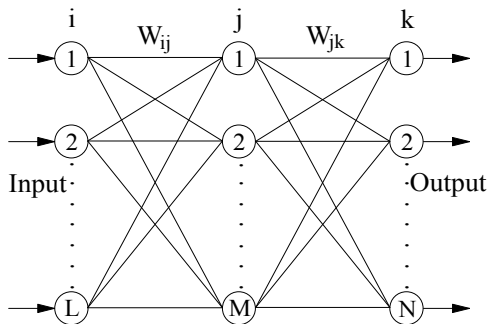
Figure 2. A three-layer neural network structure.

6.1. The Levenberg-Marquardt Algorithm

While back propagation with gradient descent technique is a steepest descent algorithm, the Levenberg−Marquardt algorithm is an approximation to Newton's method [24]. If we have a function V($\underline{x}$) which we want to minimize with respect to the parameter vector $\underline{x}$, then Newton's method would be

$$\Delta \underline{x} = - \left[\nabla^2 V(\underline{x}) \right]^{-1} \nabla V(\underline{x}) \tag{6.1}$$

where $\nabla^2 V(\underline{x})$ is the Hessian matrix and $\nabla V(\underline{x})$ is the gradient. If we assume that V($\underline{x}$) is a sum of squares function

$$V(\underline{x}) = \sum_{i=1}^{N} e_i^2(x) \tag{6.2}$$

then it can be shown that

$$\nabla V(\underline{x}) = J^T(\underline{x}) \underline{e}(\underline{x}) \tag{6.3}$$

$$\nabla^2 V(\underline{x}) = J^T(\underline{x}) J(\underline{x}) + S(\underline{x}) \tag{6.4}$$

where J(x) is the Jacobean matrix and

$$S(\underline{x}) = \sum_{i=1}^{N} e_i \nabla^2 e_i(\underline{x}) \tag{6.5}$$

For the Gauss−Newton method it is assumed that $S(\underline{x}) \approx 0$, and the update (4) becomes

$$\Delta \underline{x} = [J^T(\underline{x}) J(\underline{x})]^{-1} J^T(\underline{x}) \underline{e}(\underline{x}) \tag{6.6}$$

The Marquardt−Levenberg modification to the Gauss−Newton method is

$$\Delta \underline{x} = [J^T(\underline{x}) J(\underline{x}) + \mu I]^{-1} J^T(\underline{x}) \underline{e}(\underline{x}) \tag{6.7}$$

The parameter μ is multiplied by some factor (β) whenever a step would result in an increased V($\underline{x}$). When a step reduces V($\underline{x}$), μ is divided by β. When μ is large the algorithm becomes steepest descent (with step 1/μ), while for small μ the algorithm becomes Gauss−Newton. The Marquardt−Levenberg algorithm can be considered a trust−region modification to Gauss−Newton. The key step in this algorithm is the computation of the Jacobean matrix. For the neural network−mapping problem the terms in the Jacobean matrix can be computed by a simple modification to the back propagation algorithm [25].

7. ANN AND REGRESSION ANALYSES

A program code including neural network toolbox, were written in MATLAB language for the ANN simulations. Different ANN architectures were tried using this code and the appropriate model structure was determined.

A difficult task with ANN involves choosing parameters such as the number of hidden nodes, the learning rate, and

the initial weights. Determining an appropriate architecture of a neural network for a particular problem is an important issue, since the network topology directly affects its computational complexity and its generalization capability. The optimum network geometry is obtained utilizing a trial−and−error approach in which ANN are trained with one hidden layer. It should be noted that one hidden layer could approximate any continuous function, provided that sufficient connection weights are used [26]. Here, the hidden layer node number of ANN model were determined after trying various network structures since there is no theory yet to tell how many hidden units are needed to approximate any given function. In the training stage, the adaptive learning rate and the same initial weight were used for each ANN networks. The sigmoid activation function was used for the hidden and output nodes.

The parameters considered in the study are water discharge Q, drop height h, angle in triangular sharp−crested weir θ, air entrainment rate Q_A and aeration efficiency at 20 °C E_{20}. The parameters, Q, h, and θ were used as inputs to the ANN for the estimation of Q_A and E_{20}, respectively. 72 experimental data sets were used. The model results were evaluated using the absolute relative error (ARE) and determination coefficient (R^2) statistics.

Before applying the ANN to the data, the training input and output values were normalized using Eq. (7.1)

$$a\frac{x_i - x_{min}}{x_{max} - x_{min}} + b \qquad (7.1)$$

where x_{min} and x_{max} denote the minimum and maximum of the input and output data. Different values can be assigned for the scaling factors a and b. There are no fixed rules as to which standardization approach should

be used in particular circumstances [27]. The a and b were taken as 0.6 and 0.2 herein, respectively.

Regression analyses were performed by Baylar and Bagatur [12] using the nonlinear regression (NLR) module. Empirical correlations predicting the air entrainment rate Q_A and the aeration efficiency E_{20} for the triangular sharp−crested weirs are given in Eq. (7.2) and Eq. (7.3).

$$Q_A = \left[0.171 h^{-0.293} Q^{-0.158} \left(\cos\frac{\theta}{2} \right)^{-0.172} \right]^{-4.598} \quad (7.2)$$

$$E_{20} = 1 - \left[1 + 0.149 h^{1.341} Q^{-0.280} \left(\sin\frac{\theta}{2} \right)^{-0.206} \right]^{-1} \quad (7.3)$$

where the drop height h is in meters, the water discharge Q is in cubic meters per second, and the angle in triangular sharp−crested weir θ is in degrees.

The measured air entrainment rates Q_A and aeration efficiencies E_{20} are compared with those obtained by the ANN, NLR and linear regression technique. The ARE statistics of the measured and computed Q_A values using the ANN, nonlinear regression (NLR) and linear regression (LR) models are given in Table 1. In the eighth column, the ANN (3, 10, 1) denotes an ANN model comprising 3 input, 10 hidden and 1 output layer neurons. It can be obviously seen from Table 1 that the ANN approximates measured Q_A values with a quite high accuracy. The mean ARE of the ANN, NLR and LR are 7.1%, 25.9% and 71.2%, respectively. The accuracy of the ANN seems to be better than the regression techniques. The NLR also performs better than the LR.

Table 1. The ARE statistics for the computed Q_A using ANN, NLR and LR models.

Inputs			Q_A (m³/s x 10⁻⁴)				ARE (%)		
Q (m³/s)	h (m)	θ (deg.)	Measured	ANN (3,10,1)	NLR	LR	ANN (3,10,1)	NLR	LR
0.001	0.15	45	0.40	0.59	1.62	0.36	47.1	305.4	10.1
0.001	0.30	45	4.12	4.13	4.13	5.04	0.3	0.1	22.3
0.001	0.45	45	6.66	6.51	7.12	9.72	2.3	7.0	45.9
0.001	0.60	45	8.80	8.56	10.50	14.40	2.7	19.3	63.6
0.001	0.75	45	11.85	11.64	14.18	19.08	1.8	19.6	61.0
0.001	0.90	45	15.57	16.02	18.13	23.76	2.9	16.4	52.6
0.002	0.15	45	3.67	3.67	2.68	4.45	0.1	26.9	21.2
0.002	0.30	45	6.94	7.01	6.83	9.13	1.0	1.6	31.5
0.002	0.45	45	12.30	12.50	11.79	13.81	1.6	4.2	12.3
0.002	0.60	45	20.25	19.77	17.37	18.49	2.4	14.2	8.7
0.002	0.75	45	26.79	27.07	23.46	23.17	1.0	12.4	13.5
0.002	0.90	45	32.44	32.48	29.99	27.85	0.1	7.6	14.2
0.003	0.15	45	6.04	5.92	3.60	8.54	2.0	40.4	41.3
0.003	0.30	45	8.46	8.72	9.16	13.22	3.1	8.3	56.2
0.003	0.45	45	12.07	12.96	15.83	17.90	7.4	31.1	48.3
0.003	0.60	45	20.36	19.09	23.32				
				22.58	6.2	14.5	10.9		

0.003	0.75	45	28.00	28.03	31.49	27.26	0.1	12.5	2.7
0.003	0.90	45	39.83	40.04	40.26	31.94	0.5	1.1	19.8
0.004	0.15	45	8.57	9.75	4.44	12.63	13.8	48.2	47.3
0.004	0.30	45	14.95	12.33	11.30	17.31	17.6	24.4	15.8
0.004	0.45	45	16.02	17.18	19.50	21.99	7.2	21.7	37.2
0.004	0.60	45	24.82	25.85	28.74	26.67	4.2	15.8	7.4
0.004	0.75	45	40.11	39.14	38.81	31.35	2.4	3.2	21.8
0.004	0.90	45	51.50	51.61	49.62	36.03	0.2	3.6	30.0
0.001	0.15	90	2.48	2.72	1.31	-4.09	9.7	47.1	265.0
0.001	0.30	90	4.63	4.03	3.34	0.59	12.9	27.9	87.3
0.001	0.45	90	5.98	6.53	5.77	5.27	9.2	3.6	11.9
0.001	0.60	90	9.87	9.44	8.50	9.95	4.3	13.9	0.8
0.001	0.75	90	11.56	11.81	11.48	14.63	2.2	0.7	26.5
0.001	0.90	90	12.47	12.35	14.67	19.31	1.0	17.6	54.8
0.002	0.15	90	4.29	4.08	2.17	0.00	5.0	49.4	100.1
0.002	0.30	90	5.98	6.07	5.53	4.68	1.5	7.6	21.8
0.002	0.45	90	10.72	11.17	9.54	9.36	4.2	11.0	12.7
0.002	0.60	90	17.54	16.87	14.06	14.04	3.8	19.9	20.0
0.002	0.75	90	21.27	21.64	18.99	18.72	1.7	10.7	12.0
0.002	0.90	90	26.34	26.29	24.27	23.40	0.2	7.8	11.2
0.003	0.15	90	5.64	5.68	5.64	4.08	0.8	0.0	27.6
0.003	0.30	90	7.33	7.36	7.33	8.76	0.4	0.0	19.6
0.003	0.45	90	12.64	12.36	12.64	13.44	2.2	0.0	6.4
0.003	0.60	90	18.39	18.90	18.39	18.12	2.8	0.0	1.4
0.003	0.75	90	25.95	25.22	25.95	22.80	2.8	0.0	12.1
0.003	0.90	90	31.42	31.64	31.42	27.48	0.7	0.0	12.5
0.004	0.15	90	6.60	6.48	3.59	8.17	1.9	45.6	23.8
0.004	0.30	90	9.03	10.15	9.14	12.85	12.5	1.2	42.3
0.004	0.45	90	16.92	15.76	15.79	17.53	6.9	6.7	3.6
0.004	0.60	90	21.66	22.26	23.26	22.21	2.8	7.4	2.6
0.004	0.75	90	31.25	31.02	31.42	26.89	0.7	0.5	13.9
0.004	0.90	90	42.03	42.08	40.16	31.57	0.1	4.4	24.9
0.001	0.15	135	0.65	0.29	0.81	-8.54	54.9	24.3	1414.6
0.001	0.30	135	2.88	2.57	2.05	-3.86	10.8	28.7	234.2
0.001	0.45	135	3.50	4.34	3.55	0.82	24.0	1.4	76.7
0.001	0.60	135	5.92	6.09	5.23	5.50	2.9	11.7	7.2
0.001	0.75	135	7.95	7.88	7.06	10.18	0.8	11.2	28.0
0.001	0.90	135	10.04	9.94	9.03	14.86	1.0	10.1	48.0
0.002	0.15	135	0.50	0.56	1.34	-4.46	12.1	167.3	991.2
0.002	0.30	135	4.40	4.12	3.40	0.22	6.3	22.7	94.9
0.002	0.45	135	7.11	7.32	5.87	4.90	3.0	17.4	31.0
0.002	0.60	135	9.19	9.53	8.65	9.58	3.7	5.9	4.3
0.002	0.75	135	11.11	10.66	11.68	14.26	4.1	5.2	28.4
0.002	0.90	135	11.39	11.54	14.94	18.94	1.3	31.1	66.3
0.003	0.15	135	0.30	0.59	1.79	-0.37	95.3	498.0	222.4
0.003	0.30	135	4.79	3.84	4.56	4.31	19.8	4.7	10.0
0.003	0.45	135	7.33	7.49	7.88	8.99	2.2	7.5	22.7
0.003	0.60	135	11.79	11.76	11.61	13.67	0.3	1.5	16.0
0.003	0.75	135	15.40	16.05	15.69	18.35	4.2	1.9	19.2
0.003	0.90	135	19.80	19.52	20.05	23.03	1.4	1.3	16.3
0.004	0.15	135	1.85	2.37	2.21	3.72	27.9	19.5	101.2
0.004	0.30	135	5.58	5.23	5.63	8.40	6.2	0.8	50.6
0.004	0.45	135	7.84	8.17	9.71	13.08	4.2	23.9	66.9
0.004	0.60	135	12.64	12.17	14.31	17.76	3.7	13.2	40.5
0.004	0.75	135	18.22	18.41	19.33	22.44	1.0	6.1	23.2
0.004	0.90	135	26.63	26.61	24.71	27.12	0.1	7.2	1.8

The measured and computed air entrainment rates Q_A using the ANN, NLR and LR techniques are compared in Figure 3. It can be seen from the fit line equations (assume that the equation is $y = a_o x + a_1$) that the a_o and a_1 coefficients for the ANN are respectively closer to the

1 and 0 with a higher R^2 value of 0.997 than those of the NLR and LR. The NLR seems to be much better than the LR. This confirms the ARE statistics, which were evaluated in Table 1.
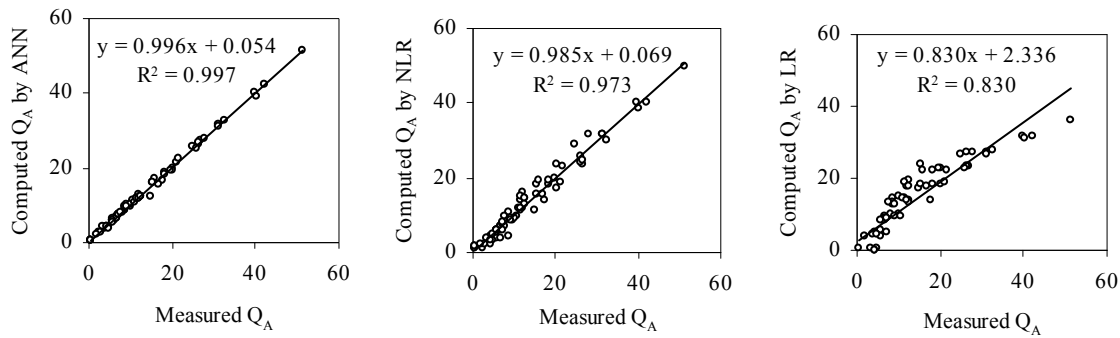

Figure 3. The comparison of measured and computed air entrainment rates Q_A using the ANN, NLR and LR techniques.

The ARE statistics for measured and computed E_{20} values are compared in Table 2. The mean ARE of the ANN, NLR and LR are 2.8%, 10.9% and 11.8%, respectively. The ANN model performs better than the NLR and LR. The mean ARE values of the NLR and LR techniques are almost equal to each other.

Table 2. The ARE statistics for the computed E_{20} using ANN, NLR and LR models.

Inputs			E_{20}				ARE (%)		
Q (m³/s)	h (m)	θ (deg.)	Measured	ANN (3,10,1)	NLR	LR	ANN (3,10,1)	NLR	LR
0.001	0.15	45	0.08	0.08	0.09	0.14	0.5	12.4	72.4
0.001	0.30	45	0.21	0.21	0.20	0.21	0.9	4.7	1.1
0.001	0.45	45	0.29	0.29	0.30	0.29	1.4	3.9	1.2
0.001	0.60	45	0.35	0.37	0.39	0.36	4.7	10.8	3.1
0.001	0.75	45	0.47	0.45	0.46	0.44	4.0	1.9	7.4
0.001	0.90	45	0.50	0.50	0.52	0.51	0.2	4.4	1.9
0.002	0.15	45	0.11	0.11	0.08	0.11	1.9	31.6	3.3
0.002	0.30	45	0.17	0.18	0.17	0.19	6.1	0.5	10.6
0.002	0.45	45	0.26	0.25	0.26	0.26	5.3	0.8	0.9
0.002	0.60	45	0.34	0.33	0.34	0.34	1.5	0.9	1.0
0.002	0.75	45	0.40	0.42	0.41	0.41	4.8	3.3	2.7
0.002	0.90	45	0.46	0.45	0.47	0.49	1.2	2.9	5.5
0.003	0.15	45	0.09	0.09	0.07	0.09	5.4	24.8	0.8
0.003	0.30	45	0.16	0.16	0.16	0.16	0.8	2.9	2.3
0.003	0.45	45	0.22	0.22	0.24	0.24	0.4	9.4	8.2
0.003	0.60	45	0.31	0.30	0.32	0.31	1.9	2.5	0.7
0.003	0.75	45	0.38	0.38	0.39	0.39	0.6	1.6	1.7
0.003	0.90	45	0.42	0.42	0.45	0.46	0.1	6.0	9.8
0.004	0.15	45	0.12	0.12	0.06	0.06	4.0	47.7	45.9
0.004	0.30	45	0.18	0.18	0.15	0.14	2.7	19.4	22.6
0.004	0.45	45	0.20	0.21	0.23				
				0.21	4.6	13.1	6.8		

0.004	0.60	45	0.30	0.30	0.30	0.29	0.6	0.2	4.0
0.004	0.75	45	0.40	0.40	0.37	0.36	1.1	8.2	9.4
0.004	0.90	45	0.45	0.45	0.43	0.44	0.3	5.5	3.0
0.001	0.15	90	0.07	0.07	0.08	0.12	6.9	14.4	68.8
0.001	0.30	90	0.15	0.17	0.18	0.19	11.4	20.4	28.3
0.001	0.45	90	0.30	0.29	0.28	0.27	2.1	8.3	11.1
0.001	0.60	90	0.35	0.36	0.36	0.34	1.5	2.4	2.5
0.001	0.75	90	0.43	0.44	0.43	0.42	1.3	0.1	3.4
0.001	0.90	90	0.48	0.49	0.49	0.49	1.8	2.2	2.0
0.002	0.15	90	0.08	0.09	0.07	0.09	12.8	16.4	17.3
0.002	0.30	90	0.16	0.15	0.15	0.17	5.9	4.0	5.1
0.002	0.45	90	0.27	0.26	0.24	0.24	2.8	11.8	10.2
0.002	0.60	90	0.32	0.34	0.32	0.32	6.3	1.5	1.0
0.002	0.75	90	0.43	0.43	0.38	0.39	0.7	11.0	9.0
0.002	0.90	90	0.50	0.50	0.44	0.47	0.5	11.6	6.9
0.003	0.15	90	0.06	0.06	0.06	0.07	3.5	0.2	15.8
0.003	0.30	90	0.13	0.14	0.14	0.14	5.1	7.3	10.6
0.003	0.45	90	0.23	0.23	0.22	0.22	1.8	5.1	5.1
0.003	0.60	90	0.28	0.27	0.29	0.29	1.8	4.0	4.5
0.003	0.75	90	0.36	0.36	0.36	0.37	0.1	1.0	1.9
0.003	0.90	90	0.44	0.44	0.41	0.44	0.2	5.8	0.3
0.004	0.15	90	0.07	0.06	0.06	0.05	15.2	20.4	35.5
0.004	0.30	90	0.12	0.13	0.13	0.12	10.5	8.4	0.4
0.004	0.45	90	0.21	0.21	0.20	0.19	1.6	2.5	7.7
0.004	0.60	90	0.27	0.27	0.27	0.27	0.2	1.8	0.7
0.004	0.75	90	0.34	0.34	0.34	0.34	0.5	0.5	0.7
0.004	0.90	90	0.42	0.42	0.39	0.42	0.3	6.0	0.8
0.001	0.15	135	0.13	0.13	0.08	0.10	2.3	41.5	24.3
0.001	0.30	135	0.17	0.17	0.17	0.17	1.1	1.6	1.6
0.001	0.45	135	0.30	0.29	0.26	0.25	2.0	11.9	17.7
0.001	0.60	135	0.34	0.35	0.35	0.32	3.6	1.7	5.5
0.001	0.75	135	0.42	0.41	0.42	0.40	2.2	0.9	5.8
0.001	0.90	135	0.46	0.45	0.48	0.47	1.4	3.6	2.2
0.002	0.15	135	0.10	0.10	0.06	0.07	1.7	36.5	26.0
0.002	0.30	135	0.12	0.12	0.15	0.15	1.3	22.2	23.6
0.002	0.45	135	0.25	0.25	0.23	0.22	1.4	8.6	10.9
0.002	0.60	135	0.32	0.32	0.30	0.30	0.5	5.2	7.2
0.002	0.75	135	0.35	0.35	0.37	0.37	1.3	5.7	6.1
0.002	0.90	135	0.42	0.42	0.43	0.45	0.3	2.0	6.1
0.003	0.15	135	0.06	0.06	0.06	0.05	2.2	4.8	17.2
0.003	0.30	135	0.08	0.08	0.13	0.12	2.2	66.3	55.1
0.003	0.45	135	0.16	0.18	0.21	0.20	12.3	30.6	24.0
0.003	0.60	135	0.28	0.28	0.28	0.27	0.2	0.0	2.6
0.003	0.75	135	0.36	0.36	0.34	0.35	0.2	4.5	3.6
0.003	0.90	135	0.44	0.44	0.40	0.42	0.5	8.9	4.2
0.004	0.15	135	0.05	0.05	0.05	0.03	3.1	5.8	49.2
0.004	0.30	135	0.07	0.07	0.12	0.10	1.1	77.1	42.4
0.004	0.45	135	0.16	0.15	0.20	0.17	7.0	22.5	8.8
0.004	0.60	135	0.23	0.24	0.26	0.25	2.6	14.7	8.0
0.004	0.75	135	0.29	0.28	0.33	0.32	2.7	12.4	11.3
0.004	0.90	135	0.36	0.37	0.38	0.40	1.6	6.1	10.3

Figure 4 compares the measured and computed aeration efficiencies E_{20} using the ANN and regression techniques. It can be seen from the fit line equations that the a_o and a_1 coefficients for the ANN are respectively closer to the 1 and 0 with a higher R^2 value of 0.997 than those of the NLR and LR as found for the preceding application.
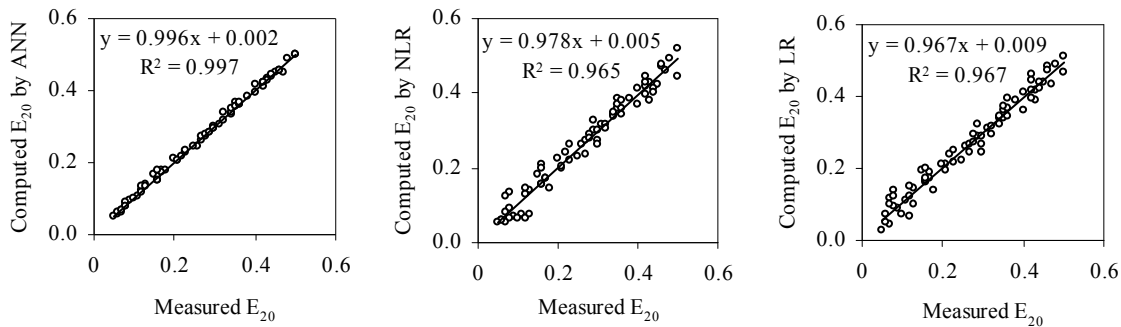
Figure 4. The comparison of measured and computed aeration efficiency E_{20} using the ANN, NLR and LR techniques.

8. CONCLUSIONS

Hydraulic structures can increase air entrainment and aeration efficiency by creating turbulent conditions where small air bubbles are carried into the bulk of the flow. Weir aeration is a particular instance of this. In this study, artificial neural network models and regression equations developed to determine the air entrainment rate and the aeration efficiency of the triangular sharp-crested weirs were compared to each other. It was found that the artificial neural network models could be successfully used in computation of air entrainment rate and aeration efficiency of weirs. Moreover, the multi nonlinear regression model was found to be better than the simple linear regression model.

REFERENCES

[1] Wilhelms, S.C., Gulliver, J.S. , Parkhill, K., "Reaeration at Low-Head Hydraulic Structures", Tech. Rep. Hl-91, *US Army Engineer Waterways Experiment Station*, Vicksburg, Miss, (1992).

[2] Chanson, H., "Predicting Oxygen Content Downstream of Weirs", Spillways and Waterways. *Proc*. Instn Civ. Engrs Wat.*, Marit. & Energy*, 112, March, 20-30 (1995).

[3] Ervine, D.A., "Air Entrainment in Hydraulic Structures: A Review", *Proc. Instn Civ. Engrs Wat., Marit. & Energy*, 130, September, 142-153 (1998).

[4] Gulliver, J.S., Wilhelms, S.C., Parkhill, K.L., "Predictive Capabilities in Oxygen Transfer at Hydraulics Structures", *J. Hydr. Engrg., ASCE*, 124 (7): 664-671 (1998).

[5] Baylar, A., Bagatur, T., "Aeration Performance of Weirs", *Water SA*, 26 (4): 521-526 (2000).

[6] Baylar, A., Bagatur, T., "Aeration Performance of Weirs", *Water Engineering & Management*, Part 1, 148 (3): 33-36 (2001).

[7] Baylar, A., Bagatur, T., "Aeration Performance of Weirs", *Water Engineering & Management*, Part 2, 148 (4): 14-16 (2001).

[8] Baylar, A., Bagatur, T., Tuna, A., "Aeration Performance of Triangular Notch Weirs at Recirculating System", *Water Quality Research Journal of Canada*, 36 (1): 121-132. (2001).

[9] Baylar, A., Bagatur, T., Tuna, A., "Aeration Performance of Triangular-Notch Weirs", *Journal of the Chartered Institution of Water & Environmental Management*, 15 (3): 203-206 (2001).

[10] Baylar, A., "Study on the Effect of Type Selection of Weir Aerators on Oxygen Transfer", Ph.D. Thesis, *Firat University,* Elazig, Turkey, (In Turkish), (2002).

[11] Baylar, A., Emiroglu, M.E., "The Effect of Sharp-Crested Weir Shape on Air Entrainment", *Canadian Journal of Civil Engineering*, 29 (3): 375-383 (2002).

[12] Baylar, A., Bagatur, T., "Experimental Studies on Air Entrainment and Oxygen Content Downstream of Sharp-Crested Weirs", *Water & Environment Journal*, 20 (4): 210-216 (2006).

[13] Gameson, A.L.H., "Weirs and Aeration of Rivers", *Journal of the Institution of Water Engineers*, 11 (5): 477-490 (1957).

[14] Ervine, D.A., McKeogh, E.J., Elsawy, E.M., "Effect of Turbulence Intensity on the Rate of Air Entrainment by Plunging Water Jets", *Proc. Instn Civ. Engrs.*, London, 69 (2): 425-445 (1980).

[15] Tsang, C.C., "Hydraulic and Aeration Performance of Labyrinth Weirs", Ph.D. Thesis, *University of London*, London, (1987).

[16] Wormleaton, P.R., Tsang, C.C., "Aeration Performance of Rectangular Planform Labyrinth Weirs", **J. Envir. Engrg., ASCE**, 126 (5): 456-465 (2000).

[17] Gameson, A.L.H., Vandyke, K.G., Ogden, C.G., "The Effect of Temperature on Aeration at Weirs", *Water & Water Engrg.*, 62, Nov., 489-492 (1958).

[18] Holler, A.G., "Reaeration of Discharge through Hydraulic Structures", Ph.D. Thesis, *University of Cincinnati*, Cincinnati, Ohio, (1970).

[19] Gulliver, J.S., Thene, J.R., Rindels, A.J., "Indexing Gas Transfer in Self-Aerated Flows", *J. Envir. Engrg.*, ASCE, 116 (3): 503-523 (1990).

[20] Levich, V.G., "Physicochemical Hydrodynamics", *Prentice-Hall*, Englewood Cliffs, N.J, (1962).

[21] Hinze, J.O., "Fundamentals of the Hydrodynamic Mechanism of Splitting in Dispersion Processes", *Am. Inst. of Chem. Eng.*, 1 (3): 289-295 (1955).

[22] Azbel, D., "Two Phase Flows in Chemical Engineering", *Cambridge Univ. Press*, Cambridge, England, (1981).

[23] Lippman, R., "An Introduction to Computing with Neural Nets", *IEEE ASSP Mag.*, 4 (2): 4-22 (1987).

[24] Marquardt, D., "An Algorithm for Least Squares Estimation of Non-Linear Parameters", *J. Soc. Ind. Appl. Math.*, 11 (2): 431-441 (1963).

[25] Hagan, M.T., Menhaj, M., "Training Feedforward Networks with the Marquardt Algorithm", *IEEE Transactions on Neural Networks*, 5 (6): 989-993 (1994).

[26] Hornik, K., Stinchcombe, M., White, H., "Multilayer Feedforward Networks are Universal Approximators", *Neural Networks*, 2 (5): 359-366 (1989).

[27] Dawson, W.C., Wilby, R., "An Artificial Neural Network Approach to Rainfall-Runoff Modeling", *Hydrol. Sci. J.*, 43 (1): 47-66 (1998).

List of Symbols

A	area of air-water interface
C	dissolved oxygen concentration
C_d	dissolved oxygen concentration downstream of a hydraulic structure
C_s	saturation concentration
C_u	dissolved oxygen concentration upstream of a hydraulic structure
DO	dissolved oxygen
D_P	bubble penetration depth
E	aeration efficiency at the water temperature of measurement
E_{20}	aeration efficiency at the 20 °C
f	exponent
h	drop height
h_t	tailwater depth
k_L	liquid film coefficient for oxygen
Q	weir discharge
Q_A	air entrainment rate
T	water temperature
t	time
t_c	air-water contact time
V	aerated volume of water
θ	angle in triangular sharp-crested weir